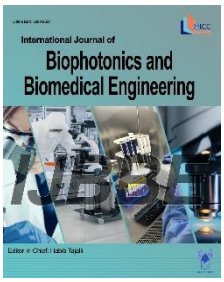

Volume 5, Issue 2, (2025) Article 12

International Journal of

Biophotonics and Biomedical Engineering (IJBBE)

https://doi.org/10.57647/ijbbe.2025.0502.12

Sonochemical Design and Characterization of 8-Hydroxyquinoline Based Nano Metal Complexes as Promising Candidates for Biomedical Engineering

Amir Safaralizadeh[1], Gholam Hossein Shahverdizadeh[1,2,*], Samad Bavili Tabrizi[1], Masoud Moghadaszadeh[3], Elnaz Ghasemi[1]

[1] *Department of Chemistry, Ta. C., Islamic Azad University, Tabriz, Iran*
[2] *Industrial Nanotechnology Research Center, Ta. C., Islamic Azad University, Tabriz, Iran*
[3] *Biotechnology Research Center, Tabriz University of Medical Sciences, Tabriz, Iran*

***Corresponding author:** shahverdizadeh@iau.ac.ir

Original Research

Received:
07 October 2025

Revised:
02 December 2025

Accepted:
16 December 2025

Published in Issue:
31 December 2025

Abstract

In this study, a new azo-quinoline derivative, 5-[(E)-(3,4- dimethylphenyl) diazenyl] quinolin-8-ol (HQ), and its zinc (II) complex [$ZnL_2(H_2O)_2$] were synthesized via a conventional route and a sonochemical approach. The HQ ligand was obtained in 75% yield (m.p. 224–226 °C), and the Zn (II) complex in 58.1% yield, both confirmed by FT-IR, UV-Vis, $^1H/^{13}C$-NMR, and elemental analyses. The sonochemical synthesis was performed using three initial ligand concentrations (0.005 M, 0.0035 M, and 0.0025 M), producing nanocomplexes with average particle sizes of 85 nm, 57 nm, and 20 nm, respectively. SEM and XRD analyses revealed that decreasing ligand concentration led to smaller, more uniform, and less agglomerated nanoparticles. The crystalline sizes estimated from XRD using the Scherer equation were consistent with SEM data. Thermal analysis (TGA/DTA) showed multi-step decomposition up to 700 °C, resulting in a stable ZnO residue. Calcination of the nanocomplex at 550–700 °C yielded ZnO nanoparticles with particle sizes of 70 nm (550 °C), 30 nm (600 °C), 65 nm (650 °C), and 60 nm (700 °C), indicating optimal morphology at 600 °C. The results demonstrate that ultrasonic irradiation and precursor concentration significantly influence particle size, crystallinity, and dispersion, highlighting the sonochemical route as a simple and efficient method for the controlled fabrication of metal–ligand nanocomplexes suitable for biomedical applications.

Keywords: Sonochemical; 8-Hydroxyquinoline derivative; Ultrasonic-assisted; Nanocomplexes

Cite this article: Safaralizadeh, A., Shahverdizadeh, Gh.H., Bavili Tabrizi, S., Moghadaszadeh, M., Ghasemi, E., Sonochemical Design and Characterization of 8-Hydroxyquinoline Based Nano Metal Complexes as Promising Candidates for Biomedical Engineering, *Int. J. Biophoton. Biomed. Eng.*, 5(2) Article 12 (2025). doi.org/10.71498/ijbbe.2025.0502.12

1. Introduction

8-Hydroxyquinoline (HQ) and its derivatives form stable chelates with a wide range of metal ions and have been widely applied in various fields. These compounds have found uses in pharmaceuticals, organic light-emitting diode (OLED) electron-transport materials, fluorescent sensor chemistry, and display significant antimicrobial,

antioxidant, anticancer, anti-inflammatory, anti-neurodegenerative, anti-malarial, and anti-tubercular activities. They have also been employed as preservatives in the textile, wood, and paper industries [1–4]. Among the HQ isomers, only 8-hydroxyquinoline forms highly stable chelates with metal ions. Its strong metal-binding ability and its capacity to modulate metal homeostasis make it useful for treating metal-related diseases. The biological activity of HQ derivatives largely depends on their strong chelating properties. Complexes based on 8-hydroxyquinoline have attracted considerable attention due to their broad applications in coordination chemistry. Azo dyes derived from 8-hydroxyquinoline play a key role in complex formation and in the detection of various metal ions, in addition to showing antibacterial activity [2–7]. Metal-ligand coordination complexes have been extensively studied due to their wide range of structural diversity and functional applications. These complexes exhibit promising performance catalysis, optoelectronics, sensing, drug delivery, and antimicrobial activity. In recent years, the downscaling of coordination compounds to the nanometer scale has attracted growing interest, as nanostructured complexes often demonstrate enhanced surface reactivity, improved solubility, and increased biological efficacy compared to their bulk analogs [3-8].

Among various metal-based nanocomplexes, zinc(II) complexes have received particular attention due to their low toxicity, biocompatibility, and rich coordination chemistry. Zinc ions can form stable complexes with a variety of organic ligands, including Schiff bases, amino acids, phenolic compounds, and heterocyclic molecules, thereby modulating their physicochemical and biological properties. Zinc nanocomplexes have shown potential as antimicrobial agents, anti-cancer drugs, enzyme mimetics, and fluorescent probes [8-11].

Various synthetic approaches have been reported for the preparation of metal-organic nanocomplexes, including solvothermal, hydrothermal, microwave-assisted, and chemical precipitation methods.

However, many of these techniques suffer from limitations such as long reaction times, high energy consumption, non-uniform particle sizes, and poor reproducibility [14,15].

Ultrasonic-assisted (sonochemical) synthesis has emerged as a powerful, green, and efficient alternative for the preparation of nanomaterials. The acoustic cavitation generated by ultrasonic waves creates extremely high local temperatures and pressures, which significantly accelerate reaction kinetics and promote the formation of nanoparticles with uniform sizes and controlled morphologies. Moreover, sonochemical synthesis is often carried out under mild conditions, without the need for high temperatures or complex equipment [14–16].

In the present study, we report the synthesis of zinc-based nanocomplexes using an ultrasonic-assisted method, in which the organic ligand was dissolved in ethanol and the zinc acetate precursor in water. The aqueous phase was added dropwise to the ethanolic phase under direct ultrasonic irradiation without any external stirring. The effects of ligand concentration on the morphology and particle size of the resulting nanocomplexes were investigated using scanning electron microscopy (Scheme 1).

2. Literature Review

In recent decades, nanostructured materials have attracted significant attention due to their unique physicochemical properties and wide-ranging applications in catalysis, drug delivery, sensing, environmental remediation, and materials science. Among these, metal-ligand nanocomplexes have emerged as a versatile class of coordination compounds, offering tunable structures, high surface area, and functional properties that can be tailored through appropriate choice of metal ions and organic ligands [8-10]. The design and synthesis of metal-based nanocomplexes have become increasingly important in the development of advanced materials with specific functionalities.

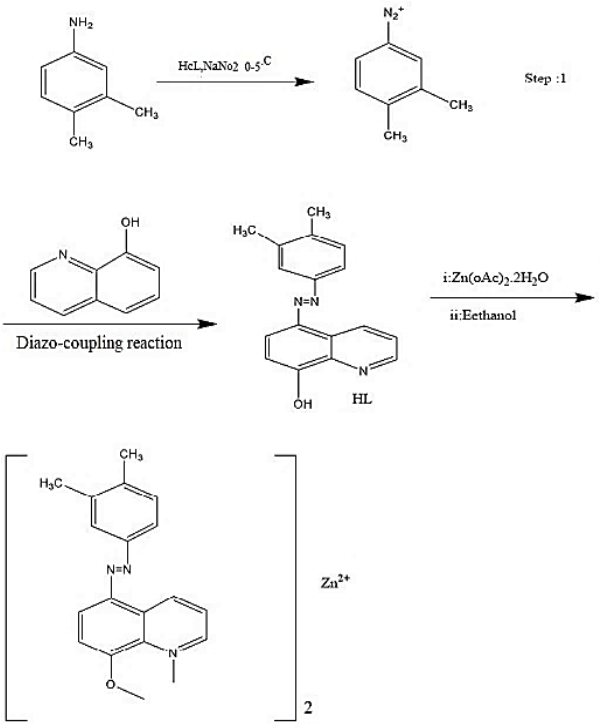

Scheme 1. illustrates the detailed synthesis procedure of the metal-ligand complex nanoparticles via ultrasonic irradiation using zinc acetate as the metal precursor and varying ligand concentrations

These nanocomplexes often exhibit superior catalytic, optical, magnetic, and biological behaviors compared to their bulk counterparts, largely due to their nanoscale dimensions and surface effects. Zinc(II)-based nanocomplexes, in particular, have been widely studied because of their low toxicity, environmental compatibility, and potential applications in biomedical and pharmaceutical fields [11-13].

3. Method

All chemical reagents and solvents were obtained from Merck Millipore (Merck KGaA, Germany) and were used as received without any further purification. Biological materials included Mueller–Hinton Broth medium (Merck, Germany) and enrofloxacin antibiotic (Sigma-Aldrich Inc.). Double-distilled water was used for the preparation of aqueous solutions.

A multi-wave ultrasonic homogenizer (Bandelin SONOPULS 3200) equipped with a KE 76 probe (BANDELIN electronic GmbH & Co., Berlin, Germany) operating at 30 kHz was used for ultrasonic irradiation at room temperature for 15 minutes in each step. FT-IR spectra were recorded using a Bruker Tensor 27 spectrophotometer. X-ray powder diffraction (XRD) patterns were obtained using a Siemens D500 powder diffractometer equipped with monochromatized Cu Kα radiation (λ = 1.54 Å). Scanning electron microscopy (SEM) images were collected using a Tescan MIRA3 FEG-SEM instrument. Thermogravimetric analysis (TGA) was carried out using a Mettler Toledo TGA/SDTA851e AG instrument in the temperature range of 10–700 °C under N_2 flow at a heating rate of 10 °C/min. UV–Vis spectra were recorded using a Shimadzu UV-1800 spectrophotometer.

3.1. Synthesis of 5-[(E)-(3,4-Dimethylphenyl) diazenyl]quinolin-8-ol (HQ) ligand

5-[(E)-(3,4-Dimethylphenyl)diazenyl]quinolin-8-ol (HQ) was synthesized from 8-hydroxyquinoline and the corresponding aniline using a conventional diazonium salt procedure, as reported in the literature [8,12,14,22]. In a 100 mL round-bottom flask, 0.5 g of 3,4-dimethylaniline was slowly dissolved in a mixture of 7 mL of distilled water and 1 mL of 37% HCl under stirring while the flask was kept in an ice bath. After 10 minutes, a clear solution was obtained. A solution of 1.5 g of sodium nitrite in 0.5 mL of cold distilled water was added dropwise to the above solution to generate the diazonium salt of 3,4-dimethylaniline. Subsequently, 0.5 mmol of 8-hydroxyquinoline dissolved in 4 mL of 10% aqueous NaOH was added dropwise to the diazonium salt solution. The optimal yield was achieved by adjusting the pH of the reaction mixture to 7–8. The resulting dark violet solution was stirred for 1 hour and then acidified with a few drops of concentrated HCl, leading to the formation of a dark brown precipitate. The solid was collected by filtration and dried under high vacuum to afford 0.16 g of the product (75% yield). Melting point: 224–226 °C.Elemental analysis calculated for C17H15N3O: C, 73.63%; H, 5.45%; N, 15.15%; found: C, 73.55%; H, 5.41%; N, 15.34%. UV-Vis (EtOH) λ_max = 361, 249 nm. FT-IR (KBr, cm^–1) selected bands: 3440 (strong), 1696 (strong), 1646 (strong), 1513 (very strong), 1384 (medium), 673 (weak), 576 (weak). ^1H NMR (DMSO-d6, δ ppm, 250 MHz): 9.31 (1H, OH), 7.10–8.97 (aromatic protons), 2.29 and 2.23 (methyl protons). ^13C NMR (DMSO-d6): 160.0, 157.5, 151.5, 149.5, 140.2, 139.2, 137.9, 132.3, 130.8, 123.6, 120.8, 114.9, 112.0, 19.8 ppm.

3.2. Preparation of $[ZnL_2(H_2O)_2]$ (1) as bulk powder

An ethanolic solution of ligand HQ (0.277 g, 1 mmol) was added dropwise to a solution of zinc acetate dihydrate (0.072 g, 0.5 mmol) in water under continuous stirring for 20 minutes. After 7 hours, the resulting mixture was filtered and washed with a water–ethanol mixture. After drying, a reddish-brick solid was obtained. *(0.094 g, yield 58.1%), m.p. > 300°C. (Anal. calc. for ZnC34H29N6O2: C, 61.73; H, 4.42; N, 12.70%; found: C, 61.69; H, 4.38; N, 12.77%). UV-Vis (EtOH) λmax = 365, 246 nm. IR (KBr, cm-1) selected bands: 3432 (s), 1697 (s), 1643 (s), 1528 (vs), 1387 (m), 669 (w), 522 (w).*

3.3. General procedure for the sonochemical synthesis of nanoparticles of $[ZnL_2(H_2O)_2]$ (1) in three different concentrations of initial reagents

Nanocomplexes were synthesized via a sonochemical route without mechanical stirring, utilizing direct ultrasonic irradiation from the beginning of the reaction. Initially, the ligand, which is readily soluble in ethanol, was dissolved in absolute ethanol to prepare stock solutions with concentrations of 0.005 M, 0.0035 M, and 0.0025 M. The solution was placed in a round-bottom flask and immediately subjected to ultrasonic irradiation using a probe-type ultrasonic device operating at a frequency of 30 kHz and a power output of 60 W. Separately, zinc acetate dihydrate was dissolved in deionized water at half the molar concentration of the ligand (0.0025 M, 0.00175 M, and 0.00125 M, respectively). The aqueous solution of zinc acetate was then slowly added dropwise to the ligand solution under continuous ultrasonic irradiation over a period of 20

minutes. No mechanical or magnetic stirring was used during the synthesis; instead, ultrasonic energy ensured efficient mixing and reaction progression. After the addition was completed and a total of 30 minutes of sonication, the resulting suspension was centrifuged at 10,000 rpm for 15 minutes to isolate the nanocomplexes. The solid products were washed several times with ethanol and deionized water to remove unreacted precursors and byproducts, and finally dried at room temperature.

3.4. Preparation of zinc oxide nanoparticles from nano complex $[ZnL_2(H_2O)_2]$ by calcination method

1 mmol of the complex $[ZnL_2(H_2O)_2]$ was placed in a porcelain crucible and calcined by heating for 2 hours at 550, 600, 650, and 700 °C. As a result of this process, zinc oxide nanoparticles were obtained.

4. Results

The FT-IR spectrum of 5-[(E)-(3,4-dimethylphenyl)diazenyl]quinolin-8-ol reveals characteristic absorption bands that confirm the presence of key functional groups within the ligand structure (Figure 1). A broad and moderately strong band observed around 3400–3450 cm^{-1} corresponds to the O–H stretching vibration of the phenolic hydroxyl group. The presence of the azo group (–N=N–) is confirmed by a sharp absorption band in the region of 1450–1500 cm^{-1}, typically associated with N=N stretching vibrations. Aromatic C–H stretching vibrations appear in the 3050–3100 cm^{-1} region, while aliphatic C–H stretches from the methyl substituents are observed around 2920–2960 cm^{-1}. Strong absorptions in the 1600–1650 cm^{-1} range are attributed to C=C stretching vibrations of the aromatic rings. Additionally, C–O stretching of the phenolic group is evident as a medium-intensity band around 1250–1280 cm^{-1}. The presence and positions of these bands are in agreement with the proposed structure of the ligand and confirm the successful synthesis of the azo-quinoline derivative.

The ^{1}H-NMR spectrum of 5-[(E)-(3,4-dimethylphenyl)diazenyl]quinolin-8-ol recorded in DMSO-d_6 exhibits chemical shifts that are consistent with the proposed molecular structure (Figure 2). A downfield singlet observed around δ ≈ 9.21–9.31 ppm corresponds to the phenolic –OH proton at the 8-position of the quinoline ring, which is deshielded due to strong intramolecular hydrogen bonding and the electron-withdrawing effect of the adjacent nitrogen atom. The aromatic protons of the quinoline moiety appear as multiple signals in the range of δ ≈ 7.10–8.97 ppm, typically displaying doublets or doublets of doublets due to ortho and meta coupling patterns, consistent with a substituted quinoline ring. The two methyl protons appear as sharp singlets around δ ≈ 2.2–2.4 ppm, each integrating for three protons, and are assigned to the CH_3 substituents at the 3- and 4-positions of the phenyl ring. The observed chemical shifts, multiplicities, and integrations are fully consistent with the expected proton environment in the proposed structure, confirming the successful synthesis and structural integrity of the ligand.

The UV–Vis. absorption spectrum of 5-[(E)-(3,4-dimethylphenyl) diazenyl] quinolin-8-ol, recorded in ethanol, exhibits distinct absorption bands characteristic of its extended conjugated π-electron system (Figure 3).

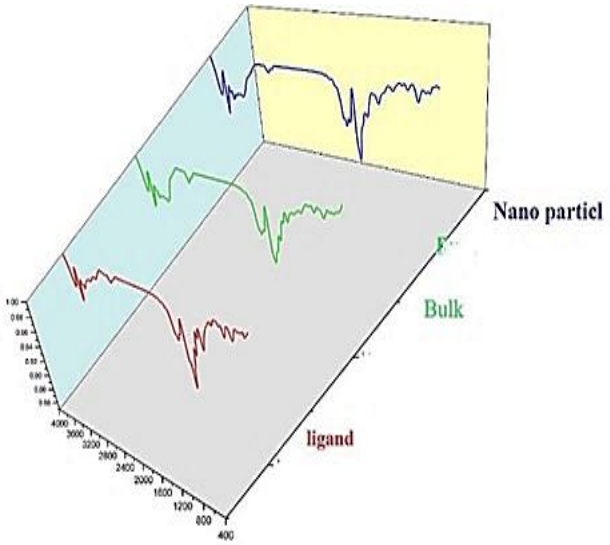

Figure 1. FT-IR spectra of (a) the HL ligand, (b) the bulk material of compound 1 as synthesized, and (c) the nano-sized form of compound 1

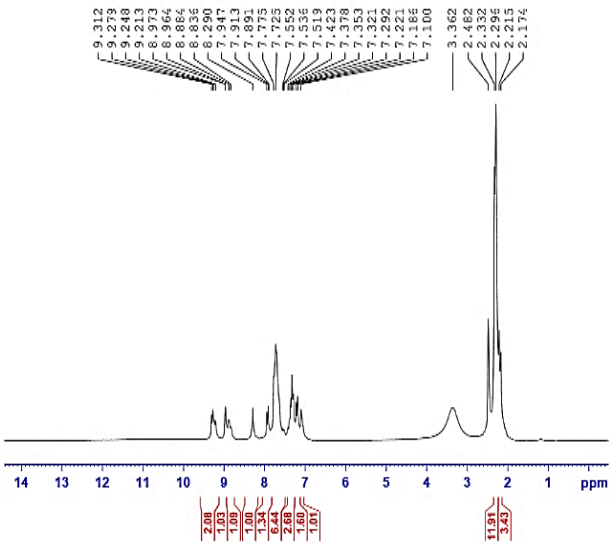

Figure 2. ^{1}HNMR spectra of HL ligand in DMSO

A strong absorption band is observed in the range of 225–365 nm, which is attributed to the π→π* transition involving the aromatic rings and the azo (–N=N–) chromophore. This transition is significantly enhanced due to the electron-donating effects of the hydroxyl group at the 8-position of the quinoline ring and the methyl substituents on the phenyl ring, which increase the electron density and conjugation across the molecule. Additionally, a less intense absorption band appears in the region of 325–420 nm, corresponding to the n→π* transition of the azo group, associated with the excitation of a non-bonding electron on the nitrogen atom to an anti-bonding π* orbital. The position of this band indicates a bathochromic shift compared to simpler azo compounds, which reflects the high degree of conjugation and intramolecular charge transfer (ICT) within the ligand structure. These spectral features confirm the presence of the azo linkage, the extended aromatic system, and the successful synthesis of the target ligand.

The FT-IR spectrum of the zinc(II) complex exhibits significant changes compared to the free ligand, confirming coordination through specific functional groups. The characteristic phenolic O–H stretching vibration, observed in the free ligand around 3200–3500 cm^{-1}, is absent in the complex spectrum, indicating deprotonation of the hydroxyl group upon coordination. The C–O stretching band, originally appearing near 1270 cm^{-1} in the ligand, shifts to lower wavenumbers in the complex, consistent with the involvement of the phenolate oxygen in Zn–O bond formation. The azo (N=N) stretching vibration, typically found between 1450 and 1500 cm^{-1}, undergoes a slight shift to lower frequencies upon complexation, suggesting coordination through the azo nitrogen atom.

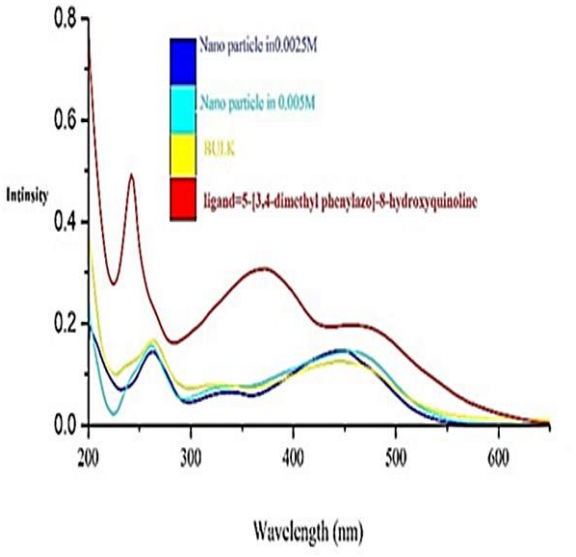

Figure 3. Comparison of UV-vis spectra of HL, Bulk, and nanoparticle

Furthermore, new absorption bands emerge in the low-frequency region around 500–600 cm^{-1}, which are assigned to Zn–O and Zn–N stretching vibrations, providing direct evidence of metal–ligand bond formation. The aromatic C=C and C=N stretching bands remain largely unaltered, confirming that coordination does not affect the aromatic ring framework. Collectively, the FT-IR data substantiate the bidentate coordination mode of the ligand to Zn(II) via the phenolate oxygen and azo nitrogen atoms, consistent with the proposed structure of the complex (Figure 1).

The ^{1}H NMR spectrum of the zinc(II) complex was recorded in DMSO-d_6 to elucidate the coordination environment and confirm ligand binding (Figure 4). Notably, the signal corresponding to the phenolic hydroxyl proton observed in the free ligand at approximately δ 9.37–9.39 ppm is absent in the complex, confirming deprotonation and coordination through the phenolate oxygen atom. The aromatic region displays multiplets between δ 6.88 and 8.69 ppm, attributable to the protons of the quinoline and substituted phenyl rings. These aromatic signals exhibit slight downfield shifts relative to the free ligand, consistent with the electron-withdrawing effect exerted by coordination to Zn(II). Additionally, the methyl protons of the 3,4-dimethylphenyl substituent resonate as singlets at δ ~2.3 ppm, maintaining their chemical environment but displaying minor shifts indicative of metal complexation. The overall pattern and integration of the signals align with the presence of two equivalent azo-quinolinolate ligands coordinated to the zinc center. The absence of exchangeable hydroxyl protons, along with the observed chemical shifts, supports the proposed bidentate coordination mode via the phenolate oxygen and azo nitrogen atoms.

The ^{13}C NMR spectrum of the zinc(II) complex was recorded in DMSO-d_6 to investigate the electronic environment of the carbon atoms upon coordination (Figure 5). The aromatic carbons of the quinoline and 3,4-dimethylphenyl rings resonate in the expected region between δ 113 and 151 ppm.

Notably, the carbon atom bonded to the phenolic oxygen (C–O) exhibits a downfield shift compared to the free ligand, appearing near δ 155–160 ppm, consistent with coordination through the phenolate oxygen and the resultant deshielding effect. Similarly, carbons adjacent to the azo (N=N) functionality display minor shifts, reflecting changes in electron density due to metal binding at the azo nitrogen. The methyl carbons of the dimethyl-substituted phenyl ring resonate at approximately δ 19.17–19.96 ppm, showing negligible shifts, which indicates that the methyl groups remain largely unaffected by coordination.

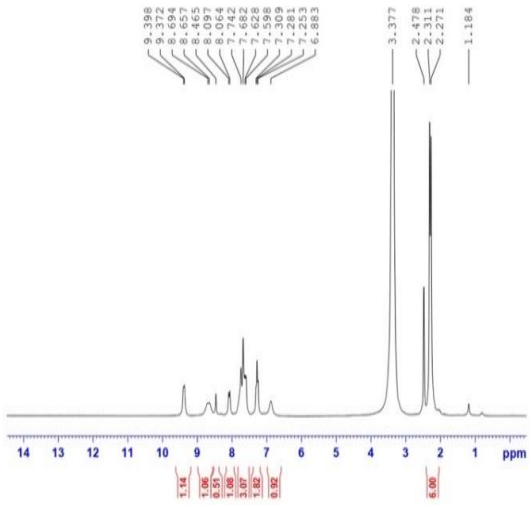

Figure 4. ^{1}H NMR spectra of HL ligand in DMSO

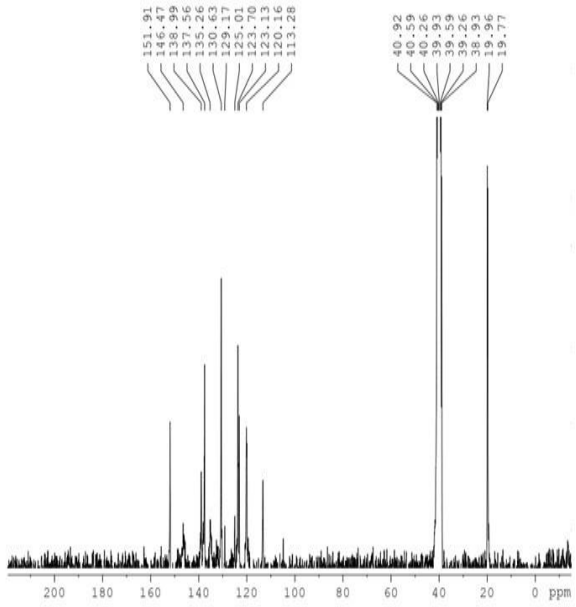

Figure 5. ^{13}C NMR spectra of $[ZnL_2(H_2O)_2]$ in DMSO

Overall, the ^{13}C spectral data corroborate the bidentate binding mode of the ligand through the phenolate oxygen and azo nitrogen atoms to the zinc center, in agreement with the proposed structure of the complex.

The UV-Vis absorption spectrum of the zinc(II) complex was recorded in an appropriate solvent to investigate the electronic transitions associated with ligand coordination. The spectrum displays intense absorption bands in the ultraviolet region around 250–290 nm, which are attributed to ligand-centered π→π* transitions involving the conjugated aromatic systems of the quinoline and phenyl rings. Additionally, a broader band observed in the range of 400–500 nm corresponds to n→π* transitions associated with the azo (–N=N–) group and intra-ligand charge transfer (ILCT) processes. Upon coordination to Zn(II), these absorption bands undergo a bathochromic shift compared to the free ligand, indicating an increase in conjugation and stabilization of the excited states due to metal–ligand interactions. Furthermore, a weaker absorption feature extending into the visible region (approximately 450–550 nm) is observed, which is assigned to ligand-to-metal charge transfer (LMCT) transitions, consistent with the involvement of the phenolate oxygen and azo nitrogen donor atoms in coordination. The overall spectral changes confirm the successful formation of the complex and provide insight into the electronic structure influenced by coordination.

The thermogravimetric analysis (TGA) of the zinc(II) complex reveals a multi-step decomposition pattern indicative of its thermal behavior and stability (Figure 6). The initial weight loss observed around 110 °C is attributed to the evaporation of physically adsorbed water molecules or residual solvents trapped within the complex matrix. This endothermic event signifies the removal of volatile impurities without affecting the complex's structural integrity. A significant weight loss occurs in the temperature range of 250–400 °C, corresponding to the decomposition of the organic azo-quinolinolate ligands. This stage involves the cleavage of the azo (–N=N–) bonds, breakdown of methyl substituents, and degradation of the aromatic quinoline and phenyl rings. The process is accompanied by substantial mass loss, indicating major ligand decomposition. Finally, in the range of 450–700 °C, a gradual and less pronounced weight loss is observed, which is associated with the further degradation of residual organic fragments and the formation of a stable inorganic residue, most likely zinc oxide (ZnO). The plateau beyond 700 °C indicates the completion of decomposition and the thermal stability of the resulting metal oxide. Overall, the TGA profile confirms the complex's moderate thermal stability and supports its proposed molecular structure.

The Differential Thermal Analysis (DTA) curve of the zinc(II) complex exhibits multiple well-defined exothermic peaks, reflecting its complex thermal decomposition mechanism. The initial exothermic peaks observed at 60 °C and 90 °C likely correspond to the release of physically adsorbed moisture or residual solvent molecules trapped within the complex lattice. These low-temperature events indicate minor thermal processes that do not significantly alter the complex's core structure. Subsequent exothermic peaks at 290 °C, 340 °C, 390 °C, and 430 °C mark the onset and progression of the primary decomposition of the organic azo-quinolinolate ligands. These peaks represent sequential oxidative breakdown of different ligand moieties, including cleavage of azo (–N=N–) bonds,

decomposition of methyl substituents, and degradation of the quinoline and phenyl aromatic rings. The multiplicity of these peaks suggests a stepwise degradation process rather than a single, concerted event. Further exothermic events at 450 °C, 480 °C, and 520 °C correspond to the continued oxidation and volatilization of residual organic fragments. These transitions reflect the progressive decomposition of more thermally stable components within the ligand framework. At higher temperatures, the exothermic peaks at 610 °C, 640 °C, and 670 °C likely indicate the final stages of decomposition, culminating in the formation of a stable inorganic residue, predominantly zinc oxide (ZnO). These high-temperature peaks are characteristic of crystallization or phase transitions of the metal oxide formed upon complete ligand degradation. Overall, the DTA profile demonstrates a complex, multi-step exothermic decomposition pathway for the zinc(II) complex, highlighting its moderate thermal stability and confirming the sequential nature of ligand breakdown and metal oxide formation. These findings complement the thermogravimetric data and provide detailed insight into the energetic processes involved in the thermal decomposition.

The morphological features and particle size distribution of the synthesized nanocomplexes were investigated using scanning electron microscopy (Figure 7). The synthesis was performed using ligand solutions at concentrations of 0.005 M, 0.0035 M, and 0.0025 M, in combination with zinc acetate at half the molar ratio of the respective ligands. The SEM images revealed that the particle size and morphology were significantly affected by the initial ligand concentration. At the highest ligand concentration (0.005 M), the resulting nanocomplexes displayed larger and more aggregated particles, with an average diameter of approximately 85 nm. This aggregation is likely due to the increased availability of ligand molecules, which can enhance coordination interactions and promote particle growth. Reducing the ligand concentration to 0.0035 M resulted in a noticeable decrease in the average particle size to approximately 57 nm. The particles appeared more discrete and moderately uniform, indicating a more controlled nucleation and growth process at this intermediate concentration. Further decreasing the ligand concentration to 0.0025 M produced significantly smaller particles, with an average diameter of about 20 nm.

The nanoparticles obtained at this concentration exhibited improved dispersity and minimal agglomeration, suggesting that lower ligand concentrations favor the formation of smaller and more stable nanostructures. Overall, the SEM analysis confirms that increasing the ligand concentration leads to the formation of larger nanocomplex particles, indicating a direct relationship between ligand concentration and particle size. These results underscore the critical role of precursor concentration in controlling the morphology and size of coordination-based nanomaterials, which is essential for tailoring their physicochemical properties for specific applications.

X-ray diffraction (XRD) analysis confirmed the crystalline nature of the obtained nanoparticles (Figure 8), and crystallite sizes estimated using the Scherrer equation were approximately 20 nm, 57 nm, and 85 nm for the ligand concentrations of 0.005 M, 0.0035 M, and 0.0025 M, respectively. The results indicate a clear inverse relationship between ligand concentration and particle size. At higher ligand concentrations, the nanoparticles were significantly smaller, likely due to the increased presence of ligand molecules acting as capping and stabilizing agents that restrict crystal growth during nucleation. The application of ultrasonic waves facilitated homogeneous nucleation and enhanced dispersion, further contributing to the formation of well-defined nanocrystals. These findings emphasize the crucial role of ligand concentration and ultrasonic energy in tuning the size and crystallinity of complex-based nanoparticles.

The influence of calcination temperature on the size and morphology of ZnO nanoparticles synthesized from compound 1 was systematically investigated at 550 °C, 600 °C, 650 °C, and 700 °C (Figure 9). The particle sizes obtained at these temperatures were approximately 70 nm, 30 nm, 65 nm, and 60 nm, respectively. Interestingly, although increasing the temperature generally enhances crystallinity, it also promotes significant particle agglomeration, particularly at higher temperatures (650 °C and 700 °C), which adversely affects the uniformity and morphology of the nanoparticles. At 600 °C, the ZnO nanoparticles exhibit the most desirable morphology, characterized by well-dispersed and uniformly sized particles with minimal agglomeration. This observation suggests that 600 °C is the optimal calcination temperature for obtaining ZnO nanoparticles with a favorable balance of particle size, dispersion, and morphological integrity.

5. Discussion

The coordination behavior of the ligand 5-[(E)-(3,4-dimethylphenyl)azo]-8-quinolinolate towards Zn(II) was elucidated through comprehensive spectroscopic analysis. The FT-IR spectrum of the complex reveals a noticeable shift of the phenolic C–O stretching vibration to lower wavenumbers relative to the free ligand, indicative of deprotonation and coordination through the phenolate oxygen.

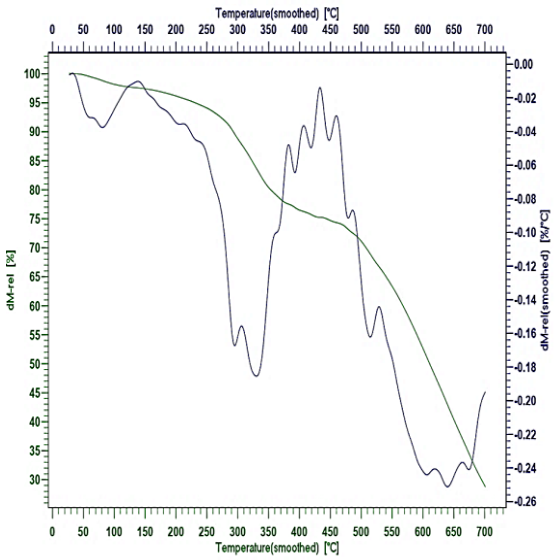

Figure 6. Thermal analysis (DTG and TGA) of the spectra of $[ZnL_2(H_2O)_2]$ in DMSO complex

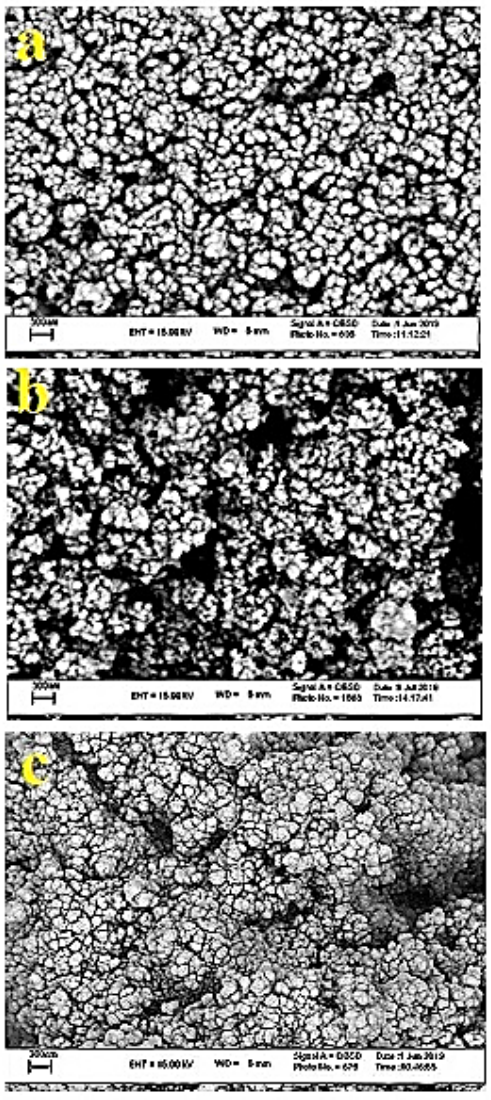

Figure 7. SEM images of nano-particles compound 1 produced by the sonochemical method in concentrations of ligand and salt: (a) 0.005:0.0025 M, (b) 0.0035:0.00175 M, (c) 0.0025:0.00125

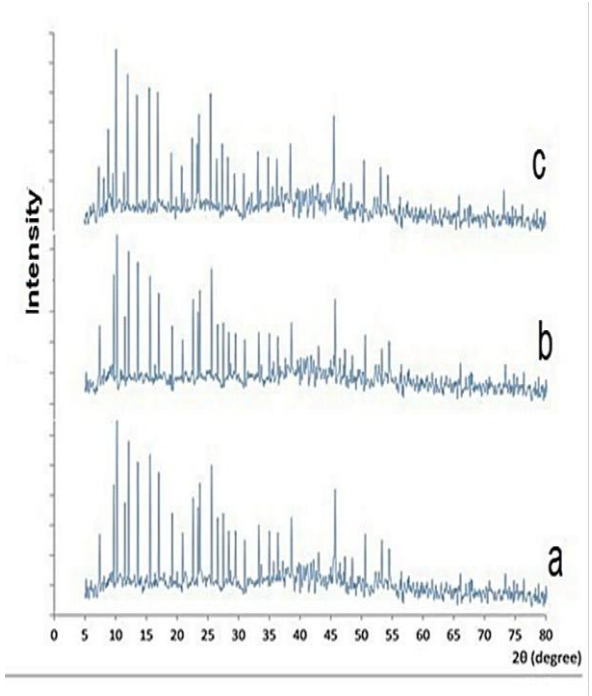

Figure 8. The XRD patterns of nanoparticles compound 1 produced by the sonochemical method in concentrations of ligand: (a) 0.005 M, (b) 0.035 M, (c) 0.0125 M

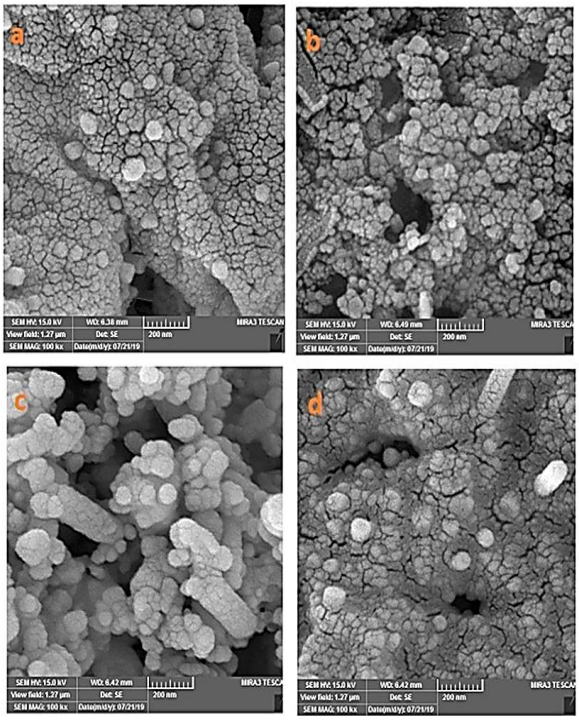

Figure 9. SEM images of ZnO nanoparticles prepared by thermal decomposition of compound 1 at (a) 550 ◦C, (b) 600 ◦C, (c) 650 ◦C, and (d) 700 ◦C

Additionally, the characteristic azo (N=N) stretching band exhibits a subtle shift, supporting involvement of the azo nitrogen in coordination. New vibrational bands observed in the 500–600 cm^{-1} region further confirm the formation of Zn–O and Zn–N bonds. The ^1H NMR spectrum displays the absence of the phenolic hydroxyl

10.57647/ijbbe.2025.0502.12

proton signal, which corroborates deprotonation upon complex formation. Aromatic proton signals experience slight downfield shifts due to the electronic influence of Zn(II) coordination, while methyl protons from the 3,4-dimethylphenyl substituent appear as sharp singlets in the expected region. Corresponding ^{13}C NMR data show minor chemical shift changes in carbons associated with the phenolic oxygen and azo functionalities, reflecting the altered electronic environment upon chelation. The UV-Vis spectrum exhibits distinct ligand-centered $\pi \rightarrow \pi^*$ transitions in the ultraviolet region alongside $n \rightarrow \pi^*$ transitions associated with the azo group. Coordination induces a bathochromic shift in these bands, which can be attributed to enhanced conjugation and metal–ligand charge-transfer interactions. Additionally, new bands appear in the visible region, likely corresponding to ligand-to-metal charge transfer (LMCT). Collectively, these spectroscopic features substantiate the bidentate coordination mode of the azo-quinolinolate ligand to Zn(II) via the phenolate oxygen and azo nitrogen atoms, confirming the successful synthesis of the complex. From a biomedical perspective, the combination of nanoscale dimensions, optical activity, and chemical stability endows these complexes with multifunctional potential. Their nanometric size facilitates cellular uptake, while the presence of 8-hydroxyquinoline a known biologically active moiety may impart intrinsic antimicrobial and antioxidant activities. Their nanometric size facilitates cellular uptake, while the presence of 8-hydroxyquinoline, a known biologically active moiety, may impart intrinsic antimicrobial and antioxidant activities. In addition, the tunable photoluminescence could be exploited for tracking and imaging within biological systems. Furthermore, the high surface-to-volume ratio allows for surface functionalization with biocompatible polymers or targeting ligands, enabling controlled drug delivery or diagnostic applications.

Overall, the results demonstrate that the sonochemical synthesis route offers a fast, controllable, and environmentally friendly pathway to produce biofunctional nanomaterials. The 8-hydroxyquinoline-based nano metal complexes synthesized in this study exhibit desirable optical, thermal, and biological properties, making them promising candidates for applications in bioimaging, targeted drug delivery, and other areas of biomedical engineering. Table 1 provides a comparative overview of different synthesis methods employed for 8-hydroxyquinoline-based metal complexes.

Table 1. Comparative study of 8-hydroxyquinoline-based metal complexes synthesized by different methods

No.	Metal Complexes	Synthetic Method	Average Particle Size (nm)	Reference
1	$[ZnI_2(H_2O)_2]$ (this work)	Sonochemical (30, kHz, 60 W)	20-85 (tunable by concentration)	Present study
2	$[Cu(L)(H_2O)]$	Conventional reflex	110	[Ref. 15]
3	$[NiL_2]$	Sol- gel	80-90	[Ref. 19]
4	$[Zn(8\text{-}HQ)_2]$	Microwave- assisted	40-60	[Ref. 21]
5	$[CoL_2(H_2O)_2]$	Ultrasonic bath (indirect)	35-50	[Ref. 22]
6	ZnO (from complex calcination, this work)	Calcination (550-700 ˚C)	30-70	Present study

6. Conclusion

In this study, metal-ligand complex nanoparticles were synthesized using zinc acetate as the precursor and varying ligand concentrations (0.005 M, 0.0035 M, and 0.0025 M, along with their half-dilutions) under ultrasonic irradiation. The results demonstrated that decreasing the ligand concentration led to the formation of smaller nanoparticles, with average sizes of approximately 85 nm, 57 nm, and 20 nm, respectively. Alongside size reduction, improved morphology and dispersion were observed at lower ligand concentrations, indicating better control over nanoparticle growth. The successful synthesis and structural properties of the nanoparticles were confirmed through comprehensive characterization using FT-IR, UV-Vis, NMR, XRD, Tg, and DTA analyses. These findings underscore the significant influence of ligand concentration on tuning both the size and morphology of metal–ligand complex nanoparticles, and they further highlight ultrasonic irradiation as an effective method for producing well-defined nanostructures.

Acknowledge

The authors would like to thank the Islamic Azad University, Tabriz Branch for providing their laboratories to support this research.

Authors Contribution

All authors have contributed equally to prepare the paper.

Availability of data and materials

The data that support the findings of this study are available from the corresponding author, upon reasonable request.

Conflict of interests

The authors declare that they have no known competing financial interests or personal relationships that could have appeared to influence the work reported in this paper.

References

[1] Jeon JH, Lee CH, Lee HS. Antimicrobial Activities of 2-Methyl-8-Hydroxyquinoline and Its Derivatives against Human Intestinal Bacteria. J Korean Soc Appl Biol Chem. 2009;52(2):202–205.
DOI: https://doi.org/10.3839/jksabc.2009.037

[2] Hegedűs, D., Szemerédi, N., Gubó, D., Spengler, G., & Szatmári, I. (2025). Synthesis, transformations and biological evaluation of 5-chloro-8-hydroxyquinoline hybrids. *European Journal of Pharmaceutical Sciences*, *209*, 107084.
DOI: https://doi.org/10.1016/j.ejps.2025.107084

[3] Shi J, Gong C, Zeng X, Zhang J, Zhu C, Xie J. Three multinuclear metal–organic coordination compounds based on 8-hydroxyquinoline derivative: Syntheses, structures and fluorescence properties. Polyhedron. 2015;102:562-568.
DOI: https://doi:10.1016/j.poly.2015.10.002

[4] Yin XD, Ma KY, Wang YL, et al. Design, synthesis, and antifungal evaluation of 8-hydroxyquinoline metal complexes against phytopathogenic fungi. J Agric Food Chem.2020;68(40):11096–11104.
DOI: https://doi:10.1021/acs.jafc.0c01322

[5] Marinova, P. E.; Tamahkyarova, K. D. Synthesis, Investigation, Biological Evaluation, and Application of Coordination Compounds with Schiff Base—A Review. Compounds 2025, 5 (2), Article 14.
DOI: https://doi.org/10.3390/compounds5020014

[6] Ramezani, B., Shahverdizadeh, G. H., Edjlali, L., Ramezani, F., & Babazadeh, M. (2020). Sonochemical synthesis of differently-sized nanoparticles of a silver(I) compound: An optical, anticancer, and thermal activity evaluation study. ChemistrySelect, 5(45), 14295–14302.
DOI: https://doi.org/10.1002/slct.202003173

[7] Ramezani B, Shahverdizadeh GH, Edjlali L, Ramezani F, Babazadeh M. Comparative study of the X-ray crystallography temperature, synthesis method, optical properties, NCI-RDG, and Hirshfeld surface analyses of coordination polymer of [CuI(DAFO)(SCN)]n: An amenable precursor for CuO nanoparticles. Sci Iran. 2023;30(6):2011-2028.
DOI: https://doi:10.24200/sci.2023.60012.6558

[8] Ghavidelaghdam, E.; Shahverdizadeh, G. H.; Motameni Tabatabai, J.; Mirtamizdoust, B. Ultrasonic-assisted synthesis of nano lead(II) coordination polymer as precursors for preparation of lead(II) oxide nano-structures: Thermal, optical properties and XRD studies. *Ultrasonics Sonochemistry* 2018, *42*, 155-161.
DOI: https://doi.org/10.1016/j.ultsonch.2017.11.007

[9] Khan, M. A.; Rizvi, M.; Siddiqui, M. A.; Malik, M. A. Zinc(II) Complexes with Schiff Bases: Synthesis, Structural Characterization, and Biological Activities. *J. Coord. Chem.* 2021, *74* (8), 1405–1420.
DOI: https://doi.org/10.1080/00958972.2021.1886504

[10] Zhou, Y.; Chen, Y.; Liu, J.; Chen, X. Zinc Coordination Polymers with Amino Acid Ligands: Synthesis, Structure, and Antibacterial Activity. *Inorg. Chem. Commun.* 2020, *119*, 107974.
DOI: https://doi.org/10.1016/j.inoche.2020.107974

[11] Patil, S. A.; Salunkhe, R. R.; Patil, P. S. Schiff Base Zinc Complexes as Fluorescent Probes: Synthesis and Photophysical Studies. *Spectrochim. Acta A Mol. Biomol. Spectrosc.* 2018, *191*, 316–324.
DOI: https://doi.org/10.1016/j.saa.2017.11.022

[12] Saadatian, M. H.; Shahverdizadeh, G. H.; Babazadeh, M.; Edjlali, L.; Es'haghi, M. The effect of ultrasonic irradiation power and initial concentration on the particle size of nano copper(II) coordination polymer: Precursors for preparation of CuO nanostructures. *Journal of Polymer Research* 2022, *29* (2), 57.
DOI: https://doi.org/10.1007/s10965-022-02913-x

[13] Saghatforoush, L. A.; Telfer, S. G.; Chalabian, F.; Mehdizadeh, R.; Golbedaghi, R.; Shahverdizadeh, G. H. Cadmium(II) complexes of 4′-tolyl-2,2′:6′,2″-terpyridine: synthesis, structures, and antibacterial activities. *Journal of Coordination Chemistry 64* (12), 2186-2201.
DOI: https://doi.org/10.1080/00958972.2011.591389

[14] Chen, Y.; Hu, M.; Wang, J.; Li, L.; Wang, Z. Sustainable Hydrothermal and Solvothermal Synthesis of Advanced Carbon Materials in Multidimensional Applications: A Review. *Materials* 2021**,** *14* (17), 5094.
DOI: https://doi.org/10.3390/ma14175094

[15] Falcaro, P.; Hill, A. J.; Nairn, K. M. S.; Jasieniak, J.; Bastow, T. J.; Slater, A. G. Synthesis and catalytic applications of metal–organic frameworks: a review on recent literature. *Int. Nano Lett.* 2018, *8*, 217-230.
DOI: https://doi.org/10.1007/s40089-018-0255-1

[16] Shahverdizadeh, G. H. From 1D chain to infinite 3D coordination polymer: sonochemical syntheses and structural characterization of a new nano lead (II) coordination compound containing three interesting coordination modes of azide anions. *Journal of Polymer Research* 2015, *22* (5), 79.
DOI: https://doi.org/10.1007/s10965-015-0725-3

[17] Ramezani, B.; Shahverdizadeh, G. H.; Edjlali, L.; Ramezani, F.; Babazadeh, M. Comparative Study of the X-ray Crystallography Temperature, Synthesis Method, Optical Properties, NCI-RDG, and Hirshfeld Surface Analyses of Coordination Polymer of [CuI(DAFO)(SCN)]n: An Amenable Precursor for CuO Nanoparticles.Sci. Iran. 2023,
DOI: https://doi.org/10.24200/sci.2023.60012.6558

[18] Shahverdizadeh, G. H.; Morsali, A. Sonochemical Synthesis of One-Dimensional Nano-structure of Three-Dimensional Cadmium(II) Coordination Polymer. *Journal of Inorganic and Organometallic Polymers and Materials* 2011, *21* (3), 694-699.
DOI: https://doi.org/10.1007/s10904-011-9468-8

[19] Cipurković, A.; Horozić, E.; Marić, S.; Mekić, L.; Junuzović, H. Metal complexes with 8-hydroxyquinoline: Synthesis and in-vitro antimicrobial activity. Open Journal of Applied Sciences 2021, 11 (1), 1–10.
DOI: https://doi.org/10.4236/ojapps.2021.111001

[20] Hao, Z. Nickel(II) complexes bearing 8-hydroxyquinoline-imine ligands: Synthesis, characterization and performance. Journal of Inorganic Biochemistry 2023, 243, 112178.
DOI: https://doi.org/10.1016/j.jinorgbio.2023.112178

[21] Al-Farhan, B. S.; Basha, M. T.; Abdel Rahman, L. H.; El-Saghier, A. M. M.; Abou El-Ezz, D.; Marzouk, A. A.; Shehata, M. R.; Abdalla, E. M. Synthesis, DFT calculations, antiproliferative, bactericidal activity and molecular docking of novel mixed-ligand salen/8-hydroxyquinoline metal complexes. Molecules 2021, 26 (16), 4725.
DOI: https://doi.org/10.3390/molecules26164725

[22] El-Lateef, H. M. A.; Khalaf, M. M.; Al-Otaibi, A. S. New mixed-ligand thioether-quinoline complexes of Co(II), Ni(II) and Cu(II): synthesis, spectral, DFT, and antimicrobial studies. Applied Organometallic Chemistry 2023, 37, e7134.
DOI: https://doi.org/10.1002/aoc.7134